

Symmetry, Structure, and Step Induced Ordering of the Si(001)-(2 × 3)Ag Surface

Thomas Michely,* Mark C. Reuter, Matt Copel, and Ruud M. Tromp

IBM Research Division, T. J. Watson Research Center, P.O. Box 218, Yorktown Heights, New York 10598

(Received 26 May 1994)

The formation of the Si(001)-(2 × 3)Ag structure has been studied by low energy electron microscopy. The lack of mirror symmetry within the (2 × 3) unit cell in the period doubled direction gives rise to the formation of two overlayer domain types on each terrace, which dynamically order with respect to step edges. We show that an anisotropic step-domain interaction energy explains the observations. Based on a quantitative determination of the number of Ag and Si atoms in the unit cell a structure model is suggested.

PACS numbers: 82.65.Dp, 68.55.Ce, 68.55.Jk, 68.55.Nq

Surface phase transitions resulting from a change in sample temperature or in the pressure of a surrounding gas phase frequency result in simultaneous growth of equivalent domains which are related by either a translation (over a fraction of the unit cell) or a rotation. Consequently, when the phase transition is completed a rather arbitrary distribution of domains results. Step edges may play a pivotal role in the nucleation and growth of these domains [1]. Here it will be demonstrated that steps may also induce a domain ordering during a surface phase transition, namely during the formation of the (2 × 3)Ag overlayer on the initially clean (2 × 1) reconstructed Si(001) surface. An anisotropic step-domain interaction turns out to be responsible for the domain ordering. The composition and structure of the (2 × 3)Ag overlayer unit cell is still controversial [2,3], resulting in part from a lack of knowledge of its composition. In this paper we present a determination of the number of Ag and Si in the unit cell, as well as the unit cell symmetry, allowing us to suggest a structure model.

The experiments have been performed in a UHV low energy electron microscope (LEEM) with a lateral resolution of 100 Å. The technique [4] and the apparatus [5] are described in detail elsewhere. In the present study we make extensive use of the excellent dark field imaging capability of the instrument. This allows the observation of image contrast based on the symmetry of the surface unit mesh. Moreover, a standard contrast mechanism in LEEM bright field imaging—the nonuniform variation of the reflection intensity for different surface features—was found to be effective also during dark field imaging. It allowed us to determine the symmetry of the unit cell, and to follow the evolution of the overlayer domain structure. A clean Si(001) surface is prepared by repeatedly heating the sample to 1300 °C. After flashing the sample was cooled to the Ag deposition temperature between 500–600 °C, just at the onset of Ag desorption. Ag was evaporated from a shutter controlled Knudsen cell with a typical Ag flux of 1 monolayer (ML) per minute arriving at the sample surface.

The clean Si(001) surface exhibits the well known (2 × 1) dimer row reconstruction, which rotates by 90° at

each single height atomic step. The low energy electron diffraction (LEED) pattern consists of the superposition of these two orthogonal (2 × 1) structures. Thus, $\frac{1}{2}$ order dark field images of the clean surface exhibit an alternating sequence of white and black terraces. Figure 1(a) shows the (2 × 3)Ag LEED pattern obtained after Ag deposition. In addition to the $\frac{1}{2}$ order spots already present before Ag deposition new streaky $\frac{1}{3}$ and $\frac{2}{3}$ order spots have appeared. Figures 1(b)–1(f) are dark field images made by selecting the diffraction spots as labeled in

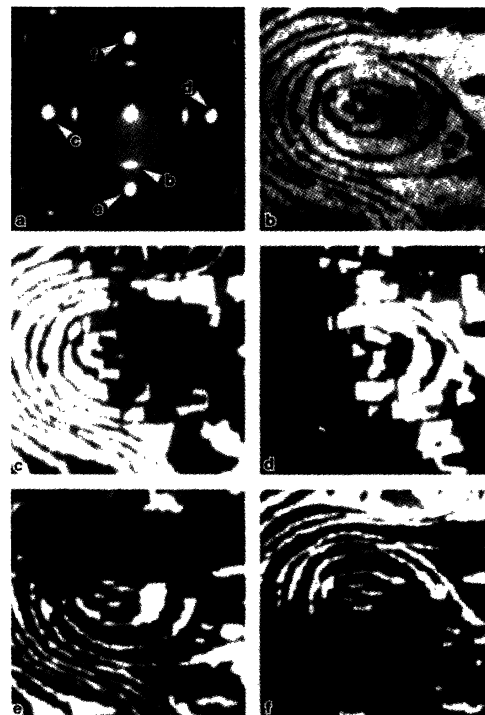


FIG. 1. Diffraction pattern of the (2 × 3)Ag overlayer on Si(001) obtained at 27 eV electron energy (a). (b)–(e) are dark field images (field of view 2.5 μm) with the image forming spots as labeled in (a). White-gray domain contrast is present in the dark field images (c)–(f) formed by $\frac{1}{2}$ spots. This contrast is absent for the image (b) formed by a $\frac{1}{3}$ order spot.

the diffraction pattern, which are $(0, -\frac{1}{3})$, $(-\frac{1}{2}, 0)$, $(\frac{1}{2}, 0)$, $(0, -\frac{1}{2})$, and $(0, \frac{1}{2})$, respectively. They all show the same circular terrace pattern of a hill on the surface [6]. On the larger terraces, especially the top terrace, a few vacancy islands of monatomic depth are visible. By comparing Fig. 1(b) with Figs. 1(c) and 1(d), which all “light up” the same terraces, it is evident that the Ag adsorption changed the periodicity along the dimer rows so that the unit mesh after adsorption is (2×3) instead of (2×1) . Ag adsorption not only changes the surface unit cell, but also the image contrast in LEEM. In Fig. 1(b), obtained with the $\frac{1}{3}$ order spot, a simple white-black contrast is present, similar to that on the clean surface. Figures 1(c)–1(f) obtained with $\frac{1}{2}$ order spots, however, exhibit an additional white-gray contrast on the bright terraces. This white-gray contrast is just complementary in Figs. 1(c) and 1(d) as well as Figs. 1(e) and 1(f). The contrast depends on electron energy and is most pronounced at 7 eV. Obviously two different LEED I - V curves contribute to the dark field image of each $\frac{1}{2}$ order spot. These images are formed by tilted-beam illumination, such that the imaging beam exists along the surface normal. The division of the bright terraces into two contrast levels indicates that tilting the beam is not a symmetry-conserving operation. In other words, the surface unit cell is asymmetric in the period doubled direction, giving rise to the formation of two types of domains. One domain type transforms into the other by a mirror operation. The absence of split contrast in Fig. 1(b) as well as in the dark field images taken with other $\frac{1}{3}$ order spots indicates that the unit cell is symmetric in the period-tripled direction. Recent scanning tunneling microscopy (STM) studies of this surface show the same asymmetry of the unit cell in the period-doubled direction [2], although it was not noticed in another STM study [3].

A closer inspection of the lateral distribution of the overlayer domains in Fig. 1 reveals a pronounced ordering with respect to step edges. To understand the nature of this ordering, we perform the following analysis. The top three layers of the surface hill in Fig. 1 are sketched in Fig. 2. Steps are solid lines, domain boundaries are dotted lines, and the asymmetry of the domains is depicted by the unit vector \mathbf{a} , defined by the imaging condition [7]. The step orientation is defined by a unit vector \mathbf{s} , orthogonal to the step in the step-up direction. With these definitions we see that the domains in Fig. 2 are distributed such that the included angle $\sphericalangle(\mathbf{a}, \mathbf{s}) \geq 90^\circ$ at any portion of a step, i.e., the scalar product $\mathbf{a} \cdot \mathbf{s}$ is minimal. This rule is generally fulfilled for any surface topography observed. To realize it, domain walls have to be created. This is especially obvious for the vacancy islands in the top terrace, where domain walls split the islands in roughly two halves. This splitting of the island terrace ensures the “right” domain orientations at the step edges. For steps nearly parallel to asymmetry vectors the domains occasionally alternate, as for instance

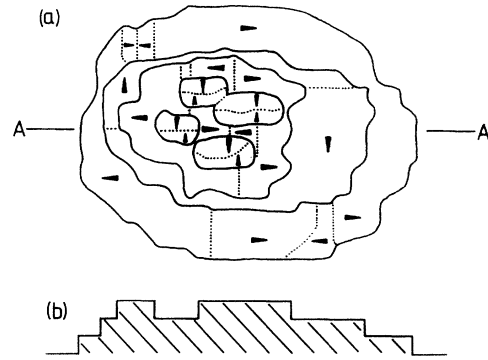


FIG. 2. Sketch of the top layers of the hill in the topography of Fig. 1(a). In (a) the asymmetry of the domains is indicated by arrows, step edges are indicated by lines and domain boundaries by dotted lines (see also text). Cross section through (a) along line A-A (b).

visible in the lower part of Fig. 2. In this case for both domain orientations $\mathbf{a} \cdot \mathbf{s} \approx 0$, so that the presence of either domain is in accord with the minimization rule formulated above. Now, assuming that the overlayer situated on a fixed step distribution is able to approach equilibrium, the domain distribution will be determined by the minimization of the free energy. The energetic terms to be considered are the interaction of the overlayer with the step edges—the domain-step interaction free energy γ_{d-s} —and the free energy γ_{d-d} needed to create the domain boundaries. This minimization then consists of (1) selecting the right domain orientation at each step edge, and (2) reducing the number and length of the domain walls. *A priori* it is not evident which of these two constraints will dominate, i.e., whether γ_{d-s} or γ_{d-d} is larger. The fact that $\mathbf{a} \cdot \mathbf{s}$ is minimized so well suggests not only that γ_{d-s} is of the form $\gamma_{d-s} = \gamma_0 \cdot \mathbf{a} \cdot \mathbf{s}$ (apart from an arbitrary constant), but also that the second constraint is of lesser importance. The coexistence of the two different domain types on every terrace allows at least the conclusion that γ_{d-d} is smaller than the difference between γ_{d-s} for the two domain types ($\gamma_{d-d} < 2\gamma_0$). In other words, a domain boundary costs less energy than the “wrong” domain asymmetry at the step edge. Since the first constraint is dominant, in order to fulfill it on any terrace a limited number of domain walls must exist (at least one). Given this, the number and length of domain walls in Fig. 2 is close to the possible minimum. Thus constraint (2) is virtually fulfilled as well. Below, we will see that the domain wall length apparent in Fig. 2 is in fact the result of a ripening process, which drastically reduces the number of domains and the domain wall length. In conclusion, the domain ordering is driven by energy minimization of the overlayer system with respect to step edges present on the surface, while simultaneously minimizing the domain boundary length.

Now we follow the dynamics of a full Ag adsorption-desorption. This will allow us to further substantiate the conclusions of the preceding analysis. To investigate simultaneously in the same experiment the role of Si in the formation of the (2×3) Ag overlayer growth, the clean Si(001) surface morphology was modified prior to Ag deposition by homoepitaxial growth. Figure 3(a) exhibits the surface after deposition of 0.53 ML Si at room temperature and subsequent ripening at elevated temperatures to form large adatom islands. During Ag deposition the Si islands are consumed [Fig. 3(b)] while the (2×3) Ag overlayer visible by the characteristic split contrast at 7 eV electron energy nucleates all over the terraces. Initially the domains are distributed almost uniformly over the surface, with only little correlation to steps. The Si adatom islands decrease continuously in size until the (2×3) Ag overlayer is complete. At that time a pattern of irregular (2×3) Ag overlayer domains is present covering the entire surface [Fig. 3(c)]. This domain pattern ripens

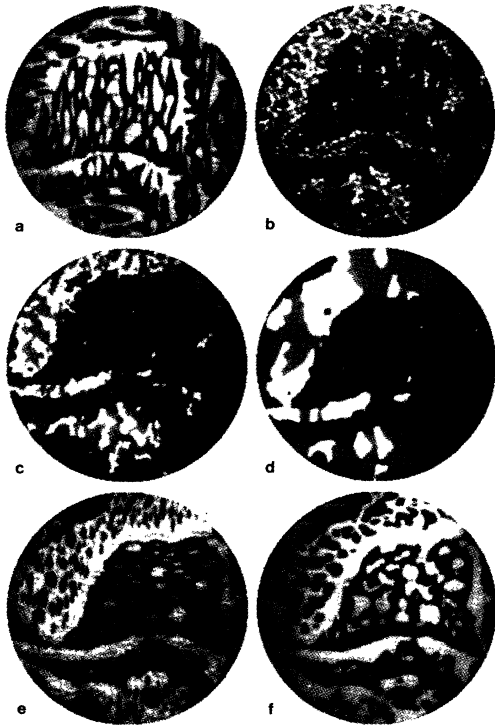


FIG. 3. Sequence of dark field images obtained with the $(\frac{1}{2}, 0)$ beam, which follows the growth and decay of the (2×3) Ag overlayer. Si adatom islands of monolayer height have been created by homoepitaxial growth prior to Ag deposition (a). Ag deposition causes nucleation of small (2×3) Ag domains (bright spots) and shrinking of adatom island sizes (b). (2×3) Ag overlayer formation has finished and island shrinking has stopped (c). The domain pattern ripens minimizing the number of domain walls (d). After closing the Ag-evaporator shutter the overlayers domains break apart and Si adatom islands grow again (e) until the entire amount of Si is recovered (f). Field of view is $4 \mu\text{m}$.

during the following minutes, thereby reducing the total domain boundary length [Fig. 3(d)]. More dramatically, during the ripening not only slow domain boundary motion is observed; occasionally large domains (up to $0.5 \mu\text{m}$ in size) flip their symmetry in a fraction of a second. Finally, when a stationary morphology results, the domain orientations present at the step edges are again consistent with the constraint to minimize γ_{d-s} , as can be checked in detail in Fig. 3(d). It appears also from Fig. 3(d), that the step-domain interaction energy γ_{d-s} is much larger than the domain energy γ_{d-d} . A great length of domain boundary is occasionally visible [e.g., white domains at the bottom of Fig. 3(d)] in order to realize the right domain orientation for a comparatively short piece of step. To prevent Ag desorption, Ag deposition continued during the entire ripening process. The excess Ag accumulates in pure Ag islands of greater thickness, which are found widely spaced on the surface (typical spacing of the order of $10 \mu\text{m}$). During Ag desorption (i.e., with the Ag evaporator shutter closed and temperature held constant) Si adatom islands reappear, exhibiting the (2×1) periodicity [Fig. 3(e)] [8]. After complete Ag desorption the amount of Si originally present in the adatom islands in Fig. 3(a) is recovered in the new adatom islands in Fig. 3(f). Several important conclusions may be drawn regarding the overlayer formation: (i) creation of the (2×3) overlayer on the clean (2×1) surface requires addition of both Ag and Si atoms to the (2×3) unit cell structure. This explains the formation of vacancy islands during (2×3) overlayer formation without Si predeposition (e.g., Fig. 1). The fact that Si is needed to create the (2×3) Ag overlayer is in clear contradiction to conclusions from previous studies [2]. (ii) Ag and Si contributing to overlayer formation are highly mobile at the sample temperature chosen, which allows the overlayer domain distribution to approach equilibrium. (iii) The dynamics of domain ordering and ripening is consistent with the assumption that they are driven by minimization of domain-step free energy and domain-wall free energy.

Finally the question of the structure of the unit cell is addressed. From several adsorption-desorption cycles with and without Si predeposition, the amount of Si needed to create a complete (2×3) Ag overlayer was measured by image analysis to be 0.52 ± 0.04 ML. *Ex situ* medium energy ion scattering (MEIS) was used to determine the amount of Ag present in the (2×3) overlayer, giving an Ag coverage of 0.54 ± 0.05 ML in the overlayer. Thus, the (2×3) overlayer contains 1 ML of material with respect to the surface density of the clean Si(001) surface, 3 Si and 3 Ag atoms in each unit cell. In the LEED pattern of Fig. 1(a) only the extra $\frac{1}{3}$ and $\frac{2}{3}$ order spots are streaky, whereas the $\frac{1}{2}$ order spots remain sharp. The streaky $\frac{1}{3}$ and $\frac{2}{3}$ order spots indicate a large number of phase shifts between overlayer rows running in the period tripled direction [2]. The sharpness of the $\frac{1}{2}$ order spots

is evidence to excellent (2×1) order on the surface. We attribute the streaky extra spots to the imperfect ordering of the adsorbed Ag decorating the well ordered (2×1) Si part of the overlayer. In addition, we find that the (2×3) overlayer transforms at room temperature and in UHV ($p < 2 \times 10^{-10}$ mbar) within 16 h to a (2×1) structure. This (2×1) structure still exhibits the same split contrast, i.e., the asymmetry is maintained, even though the triple periodicity is erased. Since it is unlikely that this change is due to room temperature motion of Si, it supports the existence of a well ordered (2×1) Si component in the (2×3) overlayer cell. Figure 4 shows a structure model for the (2×3) overlayer. The extra 3 Si atoms are adsorbed in regular lattice positions along the original (clean surface) dimer row direction, thus maintaining a well-ordered (2×1) periodicity of the Si atoms. The broken symmetry of the unit cell results from the asymmetric adsorption of Ag, which decorates the Si rows. Shifts of the Ag pattern from one row to another by a lattice vector (as indicated by the arrow in Fig. 4) give rise to the streaky appearance of the $\frac{1}{3}$ order spots in the diffraction pattern. To switch a unit cell from one asymmetry to another, only the motion of Ag atoms is required. At the temperatures under consideration (550–600 °C) at the onset of Ag desorption, Ag will also be highly mobile on the surface. The observation of the domain flip of large areas within fractions of a second as mentioned above appears thus possible for the structure model suggested here. Atomic height steps running along the top side of the unit cell (marked by an t in Fig. 4), or the bottom side of the unit cell (marked by a b), will be decorated with a different number of Ag atoms per unit length. This may be the source of the anisotropic domain-step edge interaction, giving rise to the domain ordering discussed above. While the details of this model may not

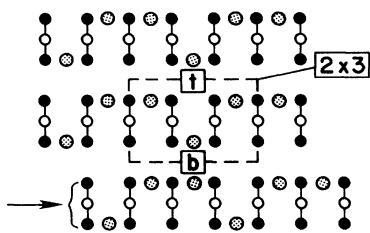


FIG. 4. Structured model for the (2×3) Ag overlayer on Si(001). Substrate Si atoms indicated as full circles, overlayer Si and Ag atoms are indicated as open and shaded circles, respectively. Top (t) and bottom (b) sides of the unit cell differ in number of Ag atoms per unit length (see also text). The (2×3) unit cells of the lower dimer row are shifted by one lattice vector in the direction indicated by the arrow.

be unique, it incorporates all the basic structural ingredients obtained above.

In summary we have used LEEM, LEED, and MEIS to determine the essential structural information on the (2×3) Ag overlayer on Si(001). The unit cell contains 3 Si and 3 Ag atoms, is composed of a well-ordered (2×1) part due to the Si in it and a decorating Ag part, which induces the period-tripling and the unit cell asymmetry in the period-doubled direction. Moreover, we have studied domain ripening and ordering with *in situ* LEEM. The processes are driven by minimization of the overlayer free energy, consisting of the domain wall energy—minimized by domain ripening—and the anisotropic domain step energy—minimized by the domain ordering with respect to step edges. We conclude that the observed domain ordering is a mesoscopic manifestation of the atomic-scale asymmetry of the (2×3) unit cell.

T. M. acknowledges a Feodor Lynen research fellowship of the Alexander von Humboldt-Foundation.

*Permanent address: Institut für Vakuumphysik und Grenzflächenforschung, Forschungszentrum Jülich, 52425 Jülich, Germany.

- [1] W. Teliëps and E. Bauer, Surf. Sci. **162**, 153 (1985); W. Swiech, E. Bauer, and M. Mundschauf, Surf. Sci. **253**, 283 (1991).
- [2] X. F. Lin, K. J. Wan, and J. Nogami, Phys. Rev. B **49**, 7385 (1994).
- [3] D. Winau, H. Itoh, A. K. Schmid, and T. Ichinokawa, Surf. Sci. **303**, 139 (1994).
- [4] W. Teliëps and E. Bauer, Ultramicroscopy **17**, 57 (1985).
- [5] R. M. Tromp and M. C. Reuter, Ultramicroscopy **36**, 99 (1991); **50**, 171 (1993).
- [6] By heating the sample to temperatures above 1000 °C while imaging with a half order spot, the central terrace of the topography in Fig. 1 shrinks until it is completely evaporated. This unambiguously establishes that the circular steps of Fig. 1 form a hill and not a crater.
- [7] The relation between \mathbf{a} and the illumination of the domain in a dark field image is as follows: Dark field imaging with a half order spot in the direction of a given asymmetry vector \mathbf{a} away from the $(0,0)$ spot will light up the domains with the asymmetry symbolized by this vector in Fig. 2.
- [8] In Fig. 3(e) the Si adatom islands have ellipsoidal shapes rotated by 90° relative to the shapes seen in Fig. 3(a), which are close to equilibrium shapes. The shape rotation is a kinetic phenomenon, present after Ag desorption. In time, the Si adatom islands ripen and change their kinetic shape towards the equilibrium shape. This shape is already nearly realized in Fig. 3(f) for a few smaller islands.

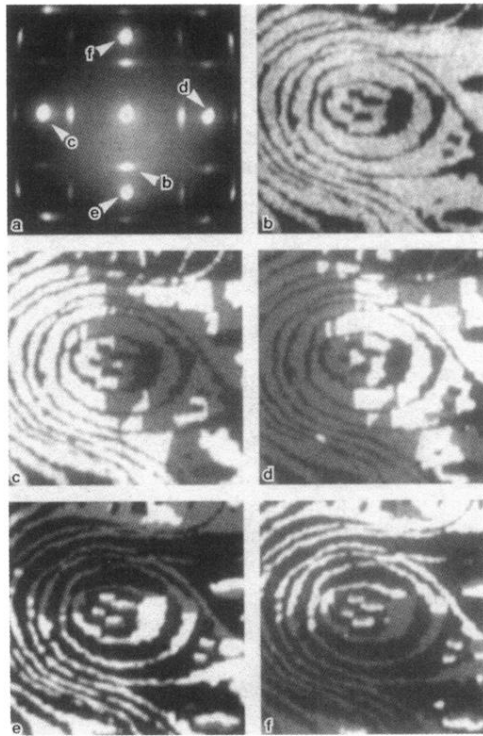


FIG. 1. Diffraction pattern of the $(2 \times 3)\text{Ag}$ overlayer on $\text{Si}(001)$ obtained at 27 eV electron energy (a). (b)–(e) are dark field images (field of view $2.5 \mu\text{m}$) with the image forming spots as labeled in (a). White-gray domain contrast is present in the dark field images (c)–(f) formed by $\frac{1}{2}$ spots. This contrast is absent for the image (b) formed by a $\frac{1}{3}$ order spot.

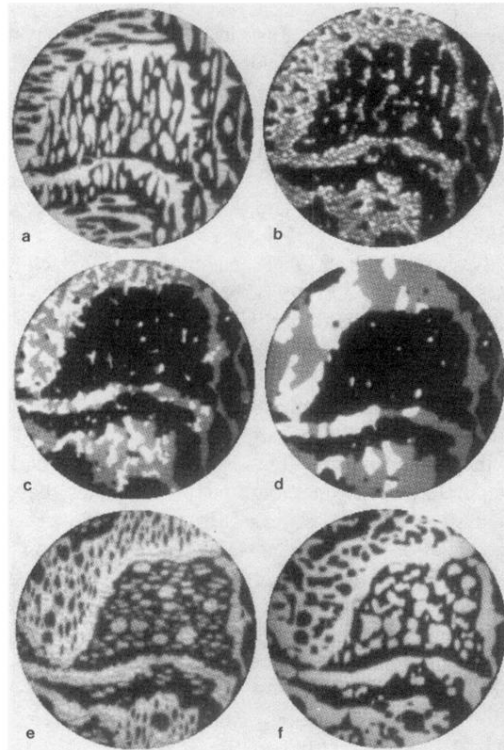


FIG. 3. Sequence of dark field images obtained with the $(\frac{1}{2}, 0)$ beam, which follows the growth and decay of the (2×3) Ag overlayer. Si adatom islands of monolayer height have been created by homoepitaxial growth prior to Ag deposition (a). Ag deposition causes nucleation of small (2×3) Ag domains (bright spots) and shrinking of adatom island sizes (b). (2×3) Ag overlayer formation has finished and island shrinking has stopped (c). The domain pattern ripens minimizing the number of domain walls (d). After closing the Ag-evaporator shutter the overlayer domains break apart and Si adatom islands grow again (e) until the entire amount of Si is recovered (f). Field of view is $4 \mu\text{m}$.

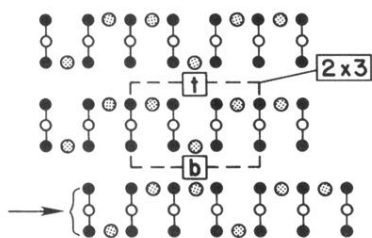


FIG. 4. Structured model for the $(2 \times 3)\text{Ag}$ overlayer on $\text{Si}(001)$. Substrate Si atoms indicated as full circles, overlayer Si and Ag atoms are indicated as open and shaded circles, respectively. Top (*t*) and bottom (*b*) sides of the unit cell differ in number of Ag atoms per unit length (see also text). The (2×3) unit cells of the lower dimer row are shifted by one lattice vector in the direction indicated by the arrow.